CHAPTER 4

Aluminum montmorillonite/polyaniline hybrid composite-based PVA organogel for removal of carcinogenic chlorophenols and congo red dye from contaminated water

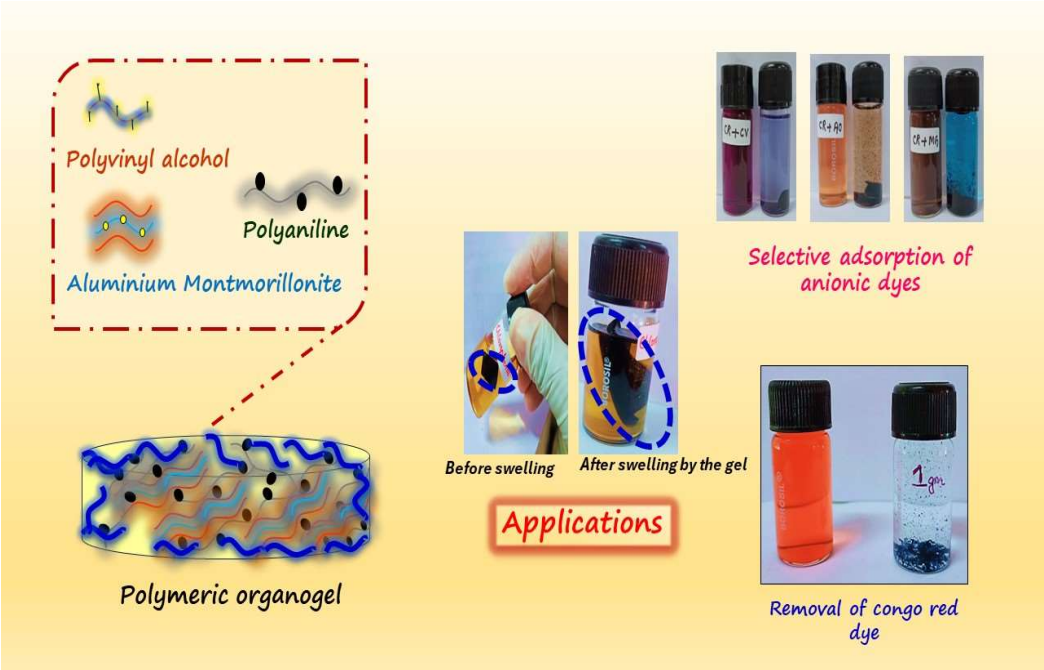

This chapter describes the formation of hybrid organogel from clay molecules in association with polyaniline to form organogels followed by its application in the removal of phenolic pollutants and selective removal of anionic dye particles.

This part of the thesis is published in

Baruah, K., Sarma, B., and Dolui, S.K. Aluminum montmorillonite/polyaniline hybrid composite-based organogel for expurgation of carcinogenic Chlorophenols and Congo red dye from defiled water sources. ***Langmuir***, 40 (1): 450-461, 2024

4.1 INTRODUCTION

With every positive aspect, inevitably comes a negative one. Industrialization has undoubtedly led to significant advancements in human development, but it has also posed serious threats to our environment, particularly concerning water resources. Various industries, such as those involved in manufacturing paints, fabrics, cosmetics, leather, and printing, heavily rely on colorants (dyes) for marketing and merchandising purposes [1]. However, the increased use of colorants has resulted in the release of toxic byproducts into aquatic ecosystems, thereby endangering the environment. These highly carcinogenic colorants disrupt the ecological balance of aquatic systems by depleting the dissolved oxygen levels in water reservoirs, thus hindering photosynthesis. Furthermore, their synthetic forms are non-biodegradable and solubility, meaning that they persist in the environment for extended periods, resulting in contamination of the aquatic systems [2,3]. In addition to colorants, industrial plants also release harmful phenols during the production of petroleum refining, plastics, resins, and solvents [4]. The ingestion of phenols is particularly dangerous, as they are mutagenic and teratogenic. Their accumulation in the environment over time has detrimental effects on both aquatic and terrestrial organisms [5].

In order to prevent industrial effluents from further polluting the environment, various remediation methods have been implemented. These methods include biological remedies, membrane filtration, advanced oxidative processes, ion exchange methods, coagulation followed by flocculation, photochemical processes, ozonation, electrochemical destruction, and absorption. However, it is worth noting that the effectiveness of these methods varies. Biological remedies, for example, have been used for a long time but are insufficient in removing complex pollutants that have emerged in recent years [6]. Advanced oxidative processes, electrochemical destruction, and ion exchange methods require the use of chemicals and continuous electricity [8,9]. Membrane filtration is prone to issues such as fouling, clogging, and the formation of sludge, all of which can impede the purification process [10]. Additionally, maintaining and repairing filtration systems can be costly and time-consuming [11]. While the photochemical process is highly efficient in degrading organic dyes [12,13], it is not suitable for treating persistent pollutants due to the presence of hydroxyl and superoxide scavenging radicals, which could pose a threat to aquatic species.

Avoiding such limitations can be achieved through a straightforward and efficient preparation method that utilizes non-toxic and cost-effective materials with high efficiency, easy productibility, and adaptiveness [14]. Adsorbents have emerged as a preferred choice for removing organic pollutants from waste resources, with various options such as polymers [17–19], graphene [20], activated carbon [21,22], MOF [23], and metal oxide-based adsorbents [24,25] being widely favored. In this work, the focus is on a non-conventional material consisting of a polymer combined with clay to form an effective adsorbent for the removal of organic dye molecules and toxic phenols.

The use of clay as a non-conventional material is advantageous due to its naturally processed nature, abundance, environmental benignity, and cost-effectiveness [26,27]. Its practical applications as catalysts, photochemical reagents, nanocomposites, and adsorbents are attributed to its large surface area, exchangeable ions, and swelling properties [28]. Among the clay minerals, Montmorillonite, which has a double-layered structure composed of a central octahedral sheet (O_h) sandwiched between two tetrahedral (T_d) silicate sheets connected by oxygen atoms, is widely used. These sheets are linked to create interlamellar spaces that can accommodate molecules [29]. Modifying the structure through size exchange with larger cations increases the interlamellar distance and basal spacing, resulting in larger pores, enhanced catalytic efficiency, exceptional surface performance, and effective ion exchange properties. The presence of metallic centers and improved thermal stability further contribute to the effective absorption of substrates [30,31]. However, the hydrolyzable nature of the cations makes the clay hydrophilic, which limits its use in large-scale manufacturing.

The significance of this work lies in its ability to address the limitations of conventional methods used to eliminate toxic organic contaminants from polluted water. The proposed method involves intercalating inorganic cations with organic cations to form hydrophobic organoclays, which have proven to be effective in removing such contaminants. Polymer materials play a crucial role in the process, providing abundant adsorbent sites [32]. To maximize efficiency, a polyaromatic compound called polyaniline (PAni) has been used. PAni is an easily synthesizable conductive polymer that offers adequate stability, environmental friendliness, and cost-effectiveness. In its polymerized state, PAni contains amine and imine groups that act as chelating agents, providing sites for adsorption from polluted sources [19-25]. The protonated amino

group of PAni interacts electrostatically with the π bonds present in dye molecules through π-π stacking.

The modification of clay minerals through the incorporation of polymeric materials between their layers leads to an enhancement in adsorption performance. This is achieved by providing additional surface area, thus increasing the availability of adsorption sites. The interaction between the intercalated polyaniline (PAni) and the lamella of the clay surface creates a synergistic effect, resulting in improved thermal stability, as well as enhanced electrical and mechanical properties [33]. Previous studies have reported on the combination of PAni with clay particles to observe mechanisms related to electrical conductivity [34,35]. However, the significance of increased surface area as an effective property for adsorption has received little attention.

In this study, a composite material based on aluminum montmorillonite and PAni, which was intercalated through in situ polymerization, was developed. The lamella structure of the clay material allows for the binding of the organic polymeric chain, resulting in a beneficial composite material with respect to the monomer used. Various compositions of clay were used to prepare the composite. Characterization of the composite was conducted using HR-XRD, FT-IR, BET, SAXS, SEM, and TGA techniques, along with rheology tests. The prepared composite was then cast to form an organogel by infusing it into polyvinyl alcohol in an organic solvent. Subsequently, the gel was employed for the absorption of organic contaminants, specifically phenolic compounds and toxic dyes. The adsorption kinetics, isothermal response, and diffusion mechanism were analyzed and investigated. The dye adsorption capacity was assessed by examining the effects of adsorbent dosage, dye concentration, and contact time. Furthermore, the removal efficiency, reusability, and separation from a mixture of dye solutions were studied.

4.2 EXPERIMENTAL SECTION

4.2.1 Materials

Aniline, Hydrochloric Acid (37%), and Dimethylsulfoxide (DMSO) were purchased from Merck. Aluminum pillared Montmorillionite (Al-MMT), and Congo Red (CR) were received from Sigma-Aldrich and Loba Chemie while Ammoniumperoxydisulphate (APS). Polyvinyl Alcohol (PVA) and p-toluenesulfonic acid (p-TSA) (98%) were procured from SRL, Otto, and BDH laboratory respectively.

Deionized water was used throughout the experiment. The reagents used were of analytical grade and used without further purification.

4.2.2 Preparation of organogel

(i) Synthesis of hybrid Clay-PAni composite

Different dosage (Table 4.1) of Al-MMT clay compound was dissolved in 100ml of water and sonicated for 8 hours to allow inflation of the clay compound. Subsequently, for in situ polymerization 0.2 M aniline was added to each solution followed by pre-cooled 1M HCL solution with additional stirring for intercalation of aniline onto the clay. An aqueous solution of 0.05 M APS was added to the mixture in drops. With an instant color change, the mixture was allowed to stand at 0 ºC with continuous stirring throughout the night. The attained deep green precipitate was filtered and washed with deionized water followed by methanol numerous times to wash away / discard removal of unreacted monomers from the mixture. The obtained product was finally dried under vacuum at 60 ºC to get the hybrid clay-PAni composite (MCP) as shown in scheme 4.1.

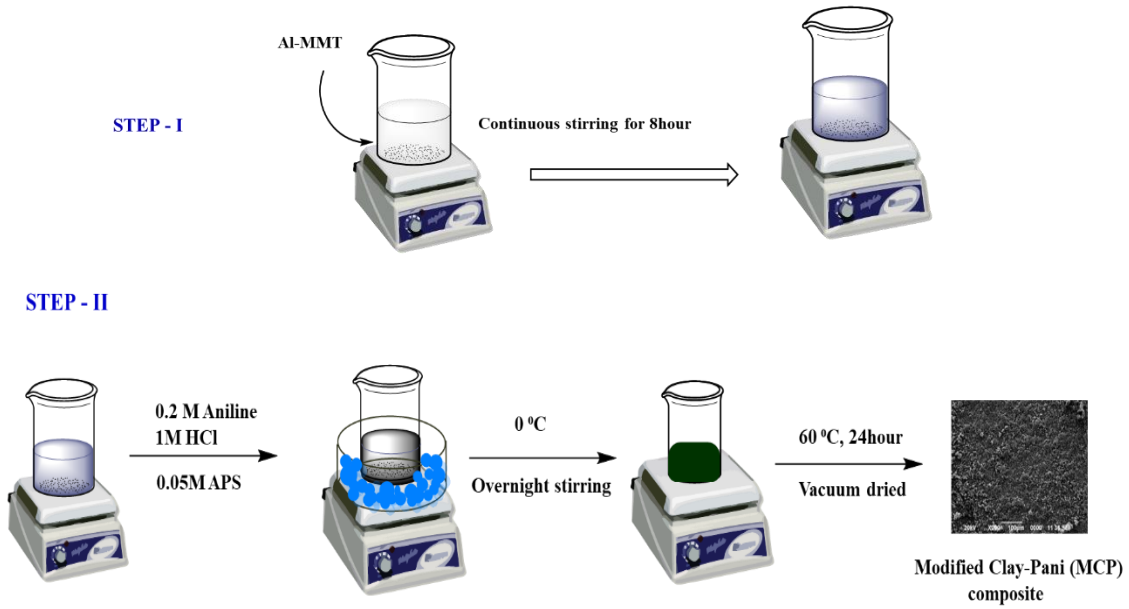

Scheme 4.1 Schematic illustration of the formation of MMT-PAni composite

(ii) Preparation of PVA-hybrid composite organogels

2.5g of PVA was dissolved in 15 mL of DMSO with the addition of *p*-TSA under continuous stirring at 80 ºC. After the dissolution of PVA molecules, prepared Clay-PAni composites of different dosages was added separately and left to stir until they completely formed a slurry compound. The formed mixture was poured onto a Petri dish

and kept under reduced pressure at 60 ºC to form gels. The gels obtained were termed PMCP (PVA-modified Clay-PAni) gels.

Table 4.1 Composition chart of prepared clay-PAni composites with peak position and d-spacing

SAMPLE	CLAY LOADING (mg)	PANI (M)	Peak position 2θ (degree)	*d*-spacing (Å)
Al-MMT	-	-	5.52	**8.01**
MCP 0.125	125	0.2	5.46	8.09
MCP 0.175	175	0.2	5.29	8.36
MCP 0.200	200	0.2	5.27	8.38
MCP 0.250	250	0.2	5.20	8.49
MCP 0.500	500	0.2	5.11	**8.65**

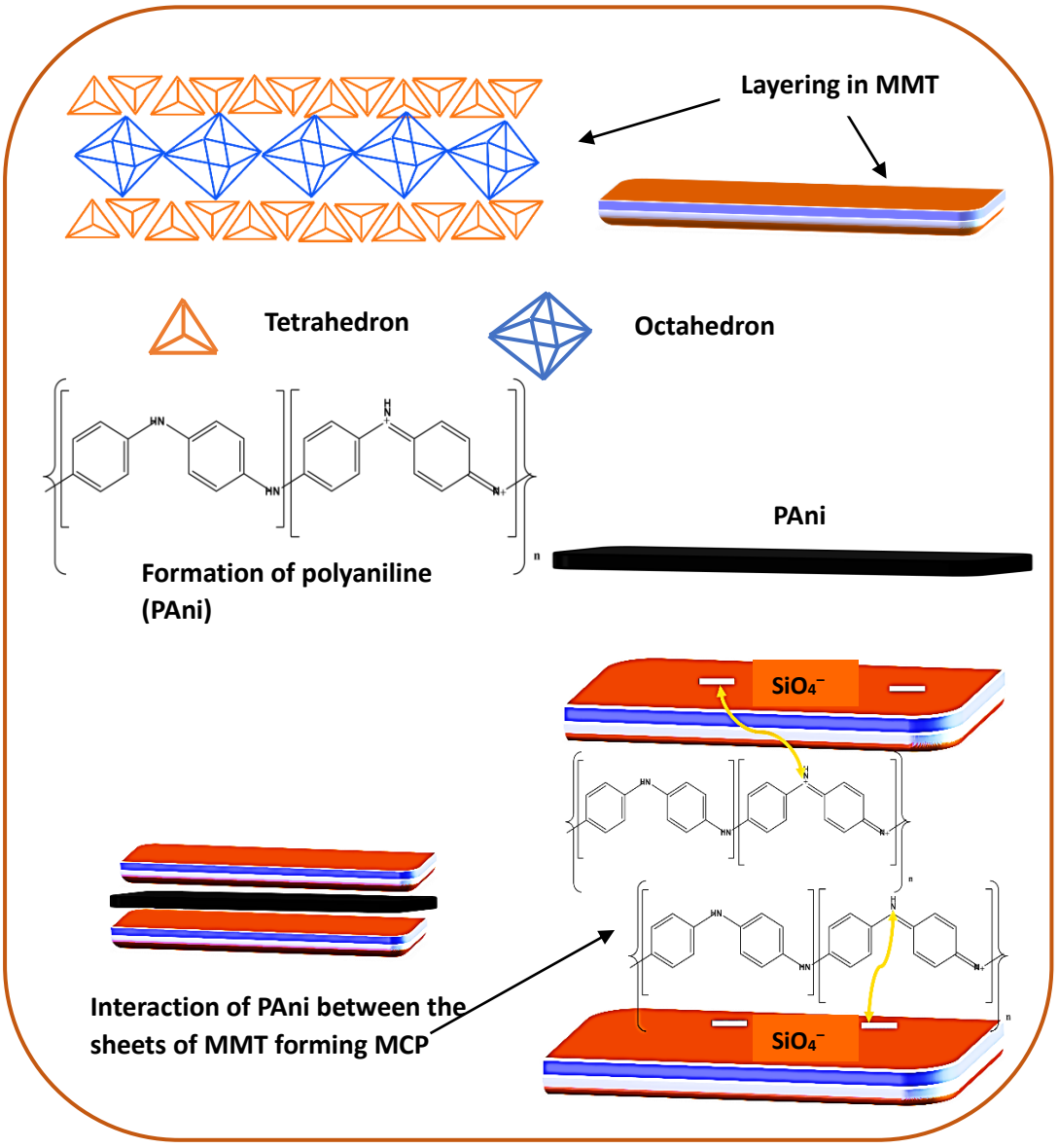

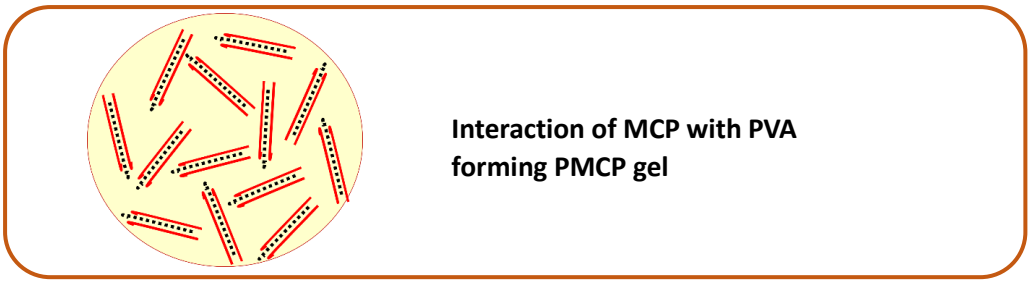

Scheme 4.2 Mechanism route to formation of MCP composite and PMCP organogel

4.2.3 Characterization

The instruments used for characterization including FT-IR, SEM, NMR, TGA, DSC and rheology tests as mentioned in section 2.2.3 of Chapter 2. The structure of the hybrid composite was investigated using a Rigaku High Resolution X-ray diffractometer, and the detection of functional groups was recorded by Nicolet Impact-410 IR (Matison, UK) spectrometer. Surface area and pore size were determined by Autosorb iQ Station 1 BET instrument. UV–Vis spectrophotometer SHIMADZU UV-2600I was used for the quantitative investigation of analytes.

4.3 RESULTS AND DISCUSSION

4.3.1 Characterization Investigation

4.3.1.1 HR-XRD analysis

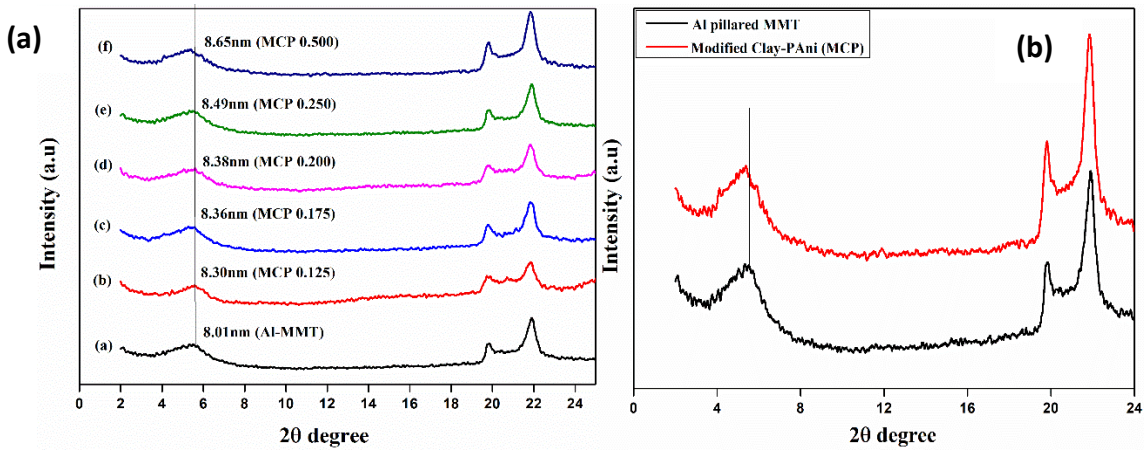

Figure 4.1 HR-XRD data of (a) prepared MCP compositions from Table 1 (b) Clay and modified composite using Ni filter

The intercalation of the PAni into the clay matrix has been distinguished by the decrease in interlayer spacing. The clay compound observed a basal spacing of 2θ value 5.52º (Figure 4.1a). The interaction of N^+ ions of PAni with the negatively charged clay surface resulted in ionic interaction causing delamination of the clay layers leading to the formation of exfoliated nanocomposite. This can be evicted from the changes visible in

the shifting of peaks. The 'abcdef' in Figure (4.1a) refers to the d-spacing of Al-MMT and clay composites. Inset captions have been added to Figure 4.1a. The d-spacing of Al-MMT increased from 8.01Å to 8.65Å with the intercalation of PAni molecules between silicate layers of clay. The HRXRD peaks for the synthesized composites are shown in Figure 4.1(b).

4.3.1.2 FT-IR analysis

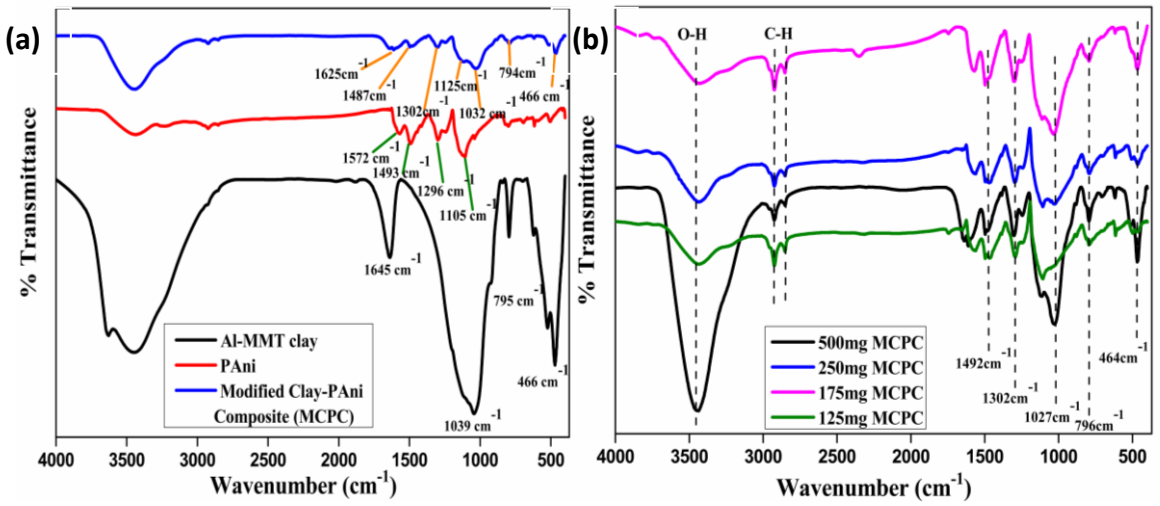

Figure 4.2 FT-IR spectra of (a) Clay, PAni, composite (b) prepared MCP composites

Figure shows the FT-IR spectra of Al-MMT, PAni, and PMCP composite. Broad bands observed in Figure 4.2(a) with 3627, 3445, and 1638 cm^{-1} depict the stretching and bending vibration of the –OH group of the lattice hydroxyl. While the 1043 cm^{-1} was observed due to the Si–O stretching present in the Al-MMT clay. 796 cm^{-1} indicates the presence of Al in the clay. In Figure 4.2(b) peaks at 1567, and 1492 cm^{-1} represent the quinoid and benzenoid rings of PAni. The vibration of the $N^{+}H$ structure formed between benzenoid and quinoid structure throughout the protonation process occurs at 1107 cm^{-1} [35]. However, Figure 4.2(a) ascribes to the peaks at 1027 cm^{-1} occurred due to the intercalation of PAni between the layers of clay. The Si–O bond was affected by the intercalant and changes in shape were evident. However, the broadening of peaks at 1611, 1027 and 794 cm^{-1} owes to the occurrence of interaction between the clay and PAni leading to the overlapping and broadening of the peaks. Figure 4.2b depicts the FT-IR bands for all the composites formed.

4.3.1.3 Morphological study

Panels a, and b from Figure 4.3 illustrate the SEM micrographs of the clay as well as of the composite. From SEM micrograph depicted in Figure 4.3a, it is evident

that the surface of the clay consists of irregularly shaped plate-like structures of varying sizes. These structures are present in different orientations and display a more curved topography. It was observed that with the in-situ polymerization of polyaniline, the clay resulted in the emergence of granular-like particles on the surface. These particles covered the plate-like structure, concealing their presence by causing aggregation of the particles. The granular particles displayed a range of sizes and shapes, with some appearing to be more spherical in nature and others being more elongated. This confirms the change in surface morphology with the intercalation of PAni between the layers of MMT.

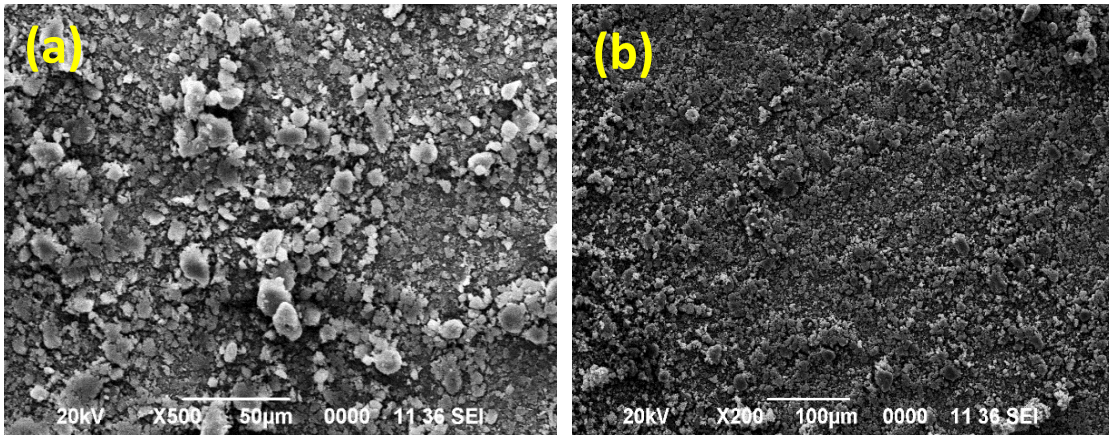

Figure 4.3 SEM micrographs of (a) Al-MMT clay (b) MCP composite

4.3.1.4 BET analysis

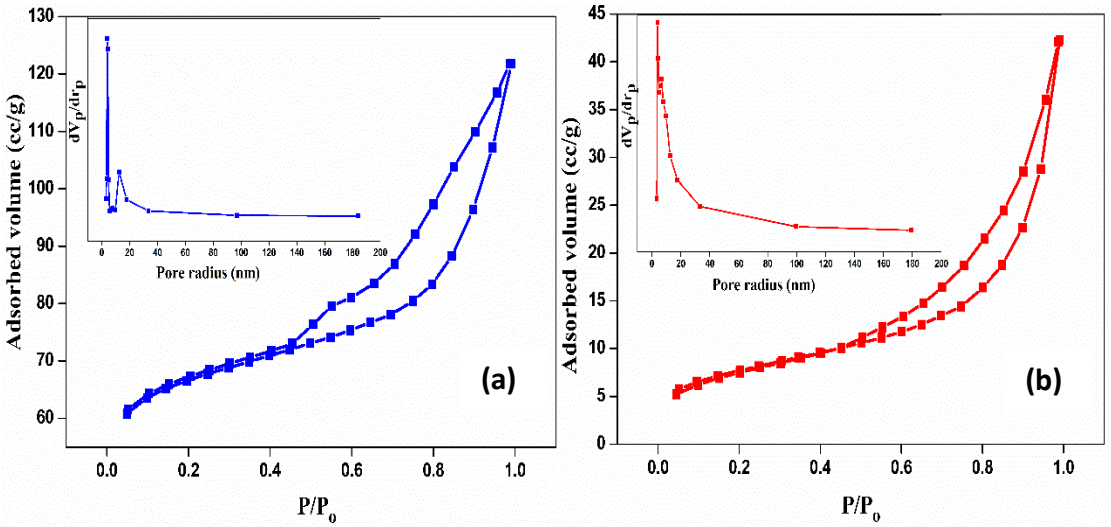

Figure 4.4 Nitrogen adsorption-desorption isotherms of (a) raw clay (b) prepared MCP composite (inset is the pore distribution graph)

The N_2 adsorption-desorption isotherm of both Al-MMT clay and the PMCP composite exhibit mesoporous characteristics resulting in Type II isotherm with monolayer adsorption. Deposition of PAni molecules on the active surface of the clay

leads to a significant reduction in its surface area from 193.78 m^2/g to 27.09 m^2/g. Simultaneously, the pore volume observed a decrease from 0.102cc/g to 0.062cc/g while the value for pore radius remained the same around 3.8nm. This decrease in surface area indicated the successful intercalation of PAni with the silicate-forming hybrid composite. Despite the changes observed in pore volume and surface area, the addition of external particles onto the clay surface kept the structure of the pore constant in both Al-MMT clay and composite. As a result, the composite retains its original pore size gained from clay with characteristics of PAni following usage in practical applications. The N_2 hysteresis loop of the clay and PMCP composite has been provided in Figure 4.4(a,b) with characteristics value in Table 4.2.

Table 4.2 Surface area, pore volume and pore size of clay and composite

SAMPLES	Surface area (m^2/g)	Pore surface area (m^2/g)	Pore size (nm)	Pore Volume (cc/g)
Al-MMT Clay	193.78	47.43	**3.88**	0.102
MCP composite	27.09	20.95	**3.86**	0.062

4.3.1.5 Thermogravimetric study

The inclusion of PAni particles onto the clay matrix greatly enhanced the properties of the composite [36]. Figure 4.5a depicts the thermogravimetric curve of the clay and PAni along with the composite formed.

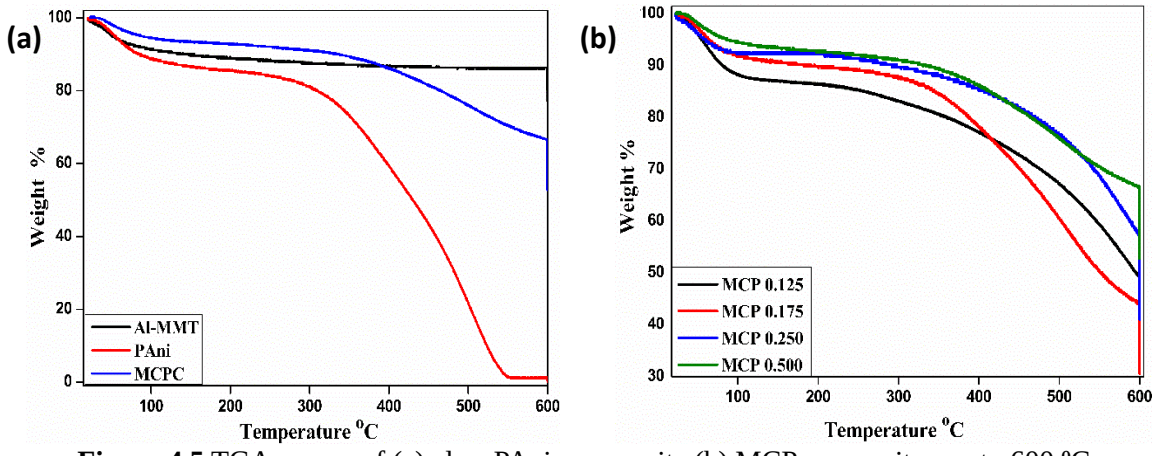

Figure 4.5 TGA curves of (a) clay, PAni, composite (b) MCP composites up to 600 ºC

The preliminary weight loss observed around 100 ºC is due to the loss of water molecules present in the composite. With 8% weight loss, the composite was stable up to around 400 ºC before the onset of degradation whereas 14% of weight loss was observed

for clay up to 400 ºC. Further, the breakage of the PAni chain was seen at 285 ºC with the complete breakdown at 550 ºC while the composite witnessed a moderate rate of degradation with only 30% of weight loss at the temperature where PAni chains ceased completely. This indicates that the PAni chains were successfully intercalated within the lamella structure of the clay nanosheets preventing degradation as well as enhancing thermal stability of the composites. The thermal degradation curve with varying compositions of the composites can be observed in Figure 4.5b.

4.3.1.6 Mechanical study

Compression tests were performed to determine the rheological properties of the prepared gel. Storage modulus indicates the ability to deform against external disturbances while loss modulus determines the flow behavior under stress. The frequency sweep experiment was carried out at room temperature at 1-10 Hz at 2% strain with a 1mm distance.

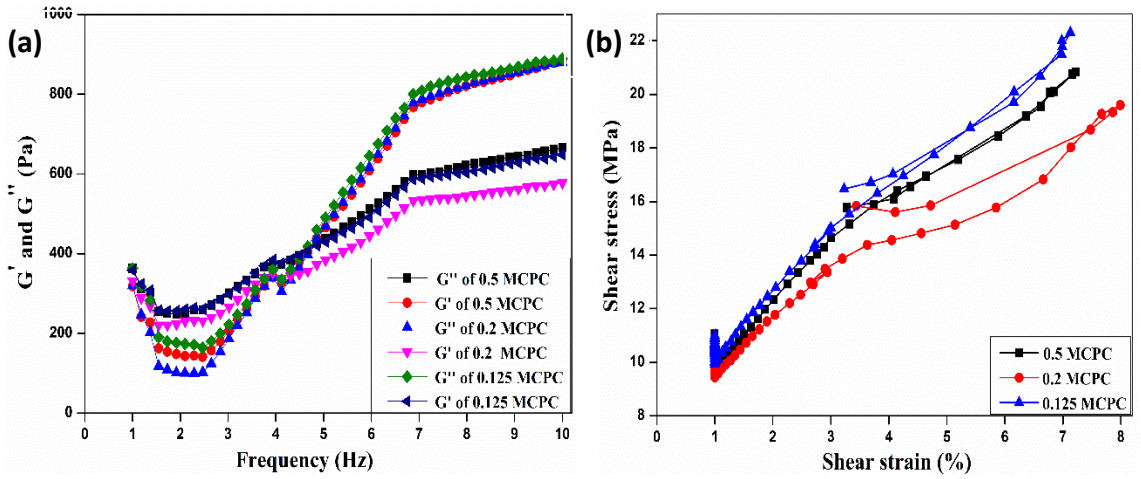

Figure 4.6 Graph of (a) Storage-Loss modulus from frequency sweep (b) Stress-strain curve of the PMCP gel with varying amount

From Figure 4.6a it can be perceived that initially there was an increase in flow behavior (G″>G′) indicating viscous property. However, at a certain frequency around 4.5Hz elastic property tends to surpass the viscous nature (G′>G″) which is termed as the cross-over frequency, also known as the Gel point. Thus, confirming the viscoelastic nature of the gel. The storage modulus was found to be 888Pa for the gel with MCP (500mg) composite. The tensile strength of the gel obtained from the stress-strain curve was found to be 20.8 Pa (Figure 4.6b). Rheological properties of other composites can be found in Figure 4.6 (a,b) respectively. The gel observed excellent stress relaxable

properties which can be observed in Figure 4.7 due to hydrogen bonding between PVA and PAni molecules within the gel structure.

Figure 4.7 The PMCP gel exhibiting excellent foldable properties and reverts back to its original shape

4.3.2 Solvent Uptake

A wide range of solvents was evaluated for the analysis of solvent uptake. Measured gravimetrically, the percent of solvent absorption was calculated using equation (i). To comprehend that the composite-based gel is highly efficient in intaking solvents: separate gels based on Aluminum montmorillonite (Al-MMT) and pure polyaniline (PAni) were prepared as described in the synthesis section. Following PVA-composite(0.5PMCP), PVA-clay and PVA-PAni gels were also prepared and their swelling properties were evaluated.

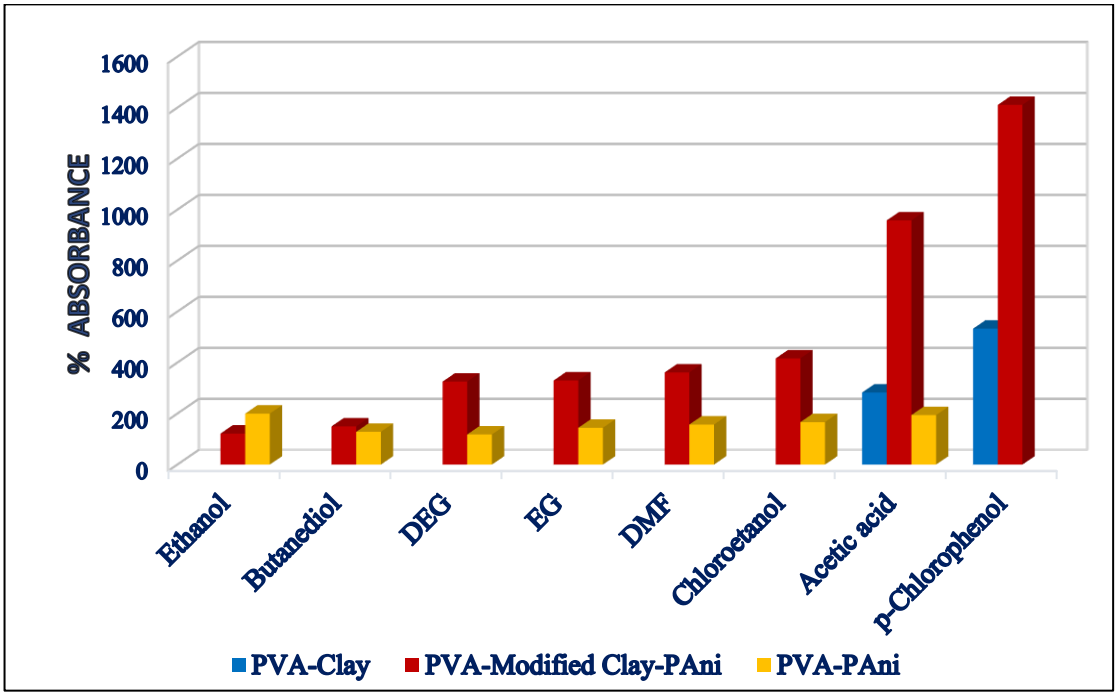

Figure 4.8 Swelling properties observed in PVA-clay, PMCP, PVA-PAni gels

The study of solvent absorption proceeded by using different solvents of raw concentration with the adsorbent. The swelling performance of the solvents were repeated thrice (where the average data has been considered for plotting of data).

Solvents used were Ethanol, Butanediol, Diethylene glycol (DEG), Ethylene glycol (EG), Chloroethanol, Acetic acid and Chlorophenol respectively.

$$\textbf{Swelling (\%)} = (W_S \div W_D) \times 100\ \% \qquad \textbf{(i)}$$

where W_S is the weight of the adsorbed sorbent and W_D is the weight of the dried/raw sorbent.

The composite-based gel was seen with high absorbable properties compared to the other two with absorbency of 1411% by *p*-chlorophenol, 958% by Acetic acid, 416% by chloroethanol, 361%, 330% and 325% by dimethylformamide, ethylene glycol, diethylene glycol respectively along with intake of 150% and 121% by butanediol and ethanol (Figure 4.8). The significant intermolecular hydrogen bonding phenomenon can be correlated with *p*-chlorophenol and acetic acid results in the expansion of the network, thereby increasing its capacity to absorb solvent. This swelling effect leads to an augmented volume of the gel and enhances its ability to intake solvent. Among the range of solvents, the composite was able to absorb around 14 times its weight of solvent p-chlorophenol. The porous structure and N^+ group obtained from the clay and PAni help the composite swell excessively and bind with the solvent, increasing its uptake percent [37-38]. The swelling analysis of the gels is shown in Table 4.3.

Table 4.3 Solvent absorption capacity by the prepared gels

SOLVENTS	PVA-Clay %	PVA-Modified Clay-Pani %	PVA-PAni %
Ethanol		121.73	200
Butanediol		150	128.57
DEG		325.64	118.18
EG		330	144.44
DMF		361.53	157.14
Chloroethanol		416.66	166.66
Acetic acid	282.62	958.06	194.11
p-Chlorophenol	533.33	**1411.11**	

Since the adsorbent was able to successfully absorb phenolic compound, different dosages of the adsorbent with varying weight percent were prepared to investigate several liquid and solid phenols including p-chlorophenol, m-Cresol, Pyrocatechol, Bisphenol A, *p*-Nitrophenol, *p*-Aminophenol. Of the mentioned solvents, the adsorbent

was able to intake only liquid phenols as the solid particles provided hindrance in entering the pores of the organogel. With 0.25 weight percent of the 0.5PMCP gel, *p*-chlorophenol exhibited swelling up to 2028%, 20 times while 839%, 8 times by *m*-Cresol. Thus, a conclusion can be drawn from the evidence that the adsorbent has impressive capability for the removal of liquid phenols from polluted sources. The absorbance percentage of chlorophenol has been shown in Figure 4.9. The swelling percent of the phenols is charted in Table 4.4.

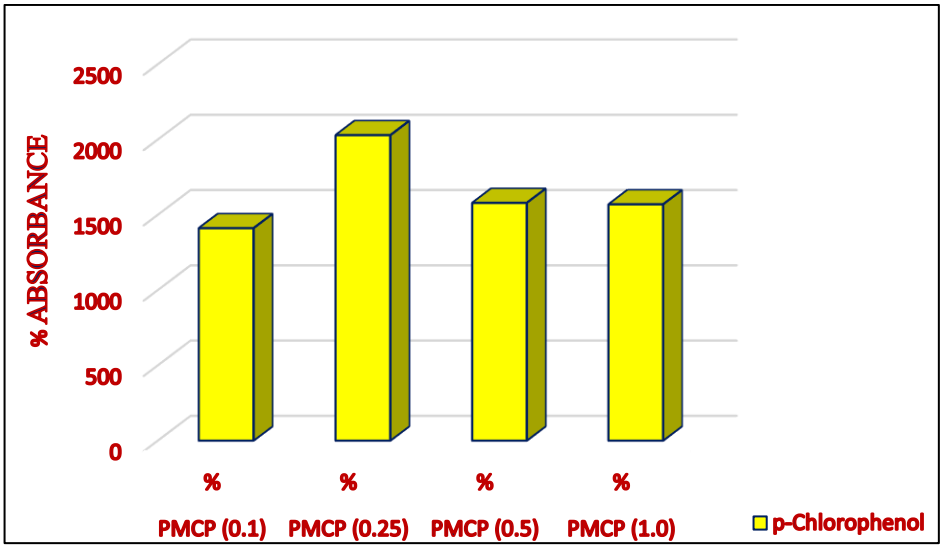

Figure 4.9 Swelling behavior of Chlorophenol in PMCP gels

Table 4.4 Absorption of phenols by PMCP gels

Absorbance % →	PMCP (0.1) %	PMCP (0.25) %	PMCP (0.5) %	PMCP (1.0) %
p-Chlorophenol	1411.11	**2028.98**	1579.18	1569.36
m-Cresol	135	**839**	257.69	182.05
Pyrocatechol	-	-	-	-
Bisphenol A	-	-	-	-
p-Nitrophenol	-	-	-	-
p-Aminophenol	-	-	-	-

4.3.2.1 Kinetics of swelling

Absorption efficiency of the solvent (*p*-chlorophenol) was investigated using kinetic study using equations (iii) and (v) from section 2.2.5 of Chapter 2. The fitted linear curves were plotted in $\ln(q_e - q_t)$ versus time and t/q_t versus time for both pseudo-first and second-order kinetics. However, linear plots were obtained for both the fitted curves with a higher regression value (R^2) of 0.97 from time versus t/q plot which

indicated that the absorption followed pseudo-second-order kinetics. The kinetic graph and table with values of k_1 and k_2 for absorption can be viewed in Figure 4.10 and Table 4.5.

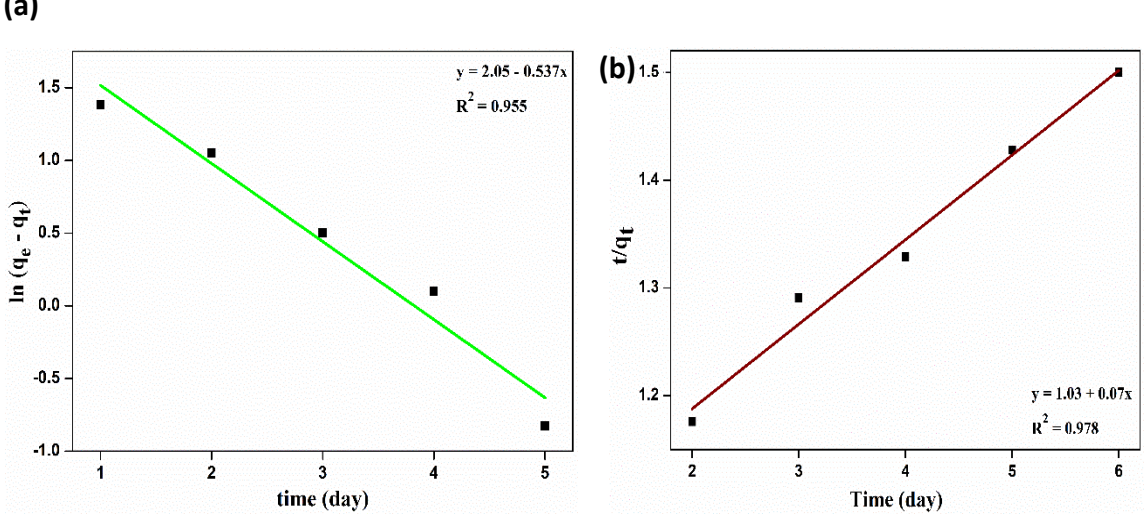

Figure 4.10 (a) The plot of ln(qe-qt) vs time for first order kinetics and (b) plot of t/qt vs time graph for second order kinetics involved in solvent absorption

Table 4.5 Parameters for kinetic models of solvent absorption

pseudo-first-order kinetics model			pseudo-second-order kinetics model		
$k_1(min^{-1})$	$Q_{max}(gg^{-1})$	R^2	$k_2(gg^{-1}min^{-1})$	$Q_{max}(gg^{-1})$	R^2
0.535×10^{-1}	1.41	**0.955**	0.597×10^{-1}	1.5	**0.978**

4.3.3 Dye adsorption

Complications with aquatic sources have arisen to a peak with the discarding of organic and synthetic dyes as they are soluble in water and persist for a longer period. To avoid further intricacy and to maximize the usage of composite particles, organogel prepared has been used as a sorbent for the removal of dye-contaminated sources. As observed from HR-XRD, PMCP (0.5) has been modified to form a gel. Congo Red (CR) has been chosen as the anionic dye. The adsorption of dye molecules has been determined using maximum peak absorbance of Congo red at approximately 498nm. The sorption process was carried out at room temperature while the analytes were measured using UV-Vis spectroscopy.

Anionic dye, Congo Red was used to observe the dye removal performance by the adsorbent. 10mg (0.1g) of the sorbent was added to 100 mL of the dye solution. The experiment was carried out at 30 ºC. Aliquots were collected at certain time intervals

until dye molecules get completely adsorbed. The experiment was repeated 5times to obtain accuracy. Similar process in different batches were carried out to study varying parameters such as dosage, concentrations, contact time, effect of pH. Absorbance spectra of the supernatant solutions were recorded using a UV-Vis spectrometer. Reusability along with the study of mixed dyes was also conducted to observe the selectivity of the adsorbent. Adsorption kinetics, as well as isothermal studies, were also conducted to obtain the mechanistic behavior of adsorption. The amount of dye adsorbed and removal efficiency of the dye was obtained using equation (ii) and (iii)

$$q_e = C_o{-}C_e/W \times V$$

$$\%\, Removal = C_o - C_e/C_o \times 100$$

where C_o and C_e represents the initial and equilibrium dye concentration, W and V is the weight of adsorbent along with volume of solution used respectively.

4.3.3.1 Effect of adsorbent dosage

The efficiency of the material to adsorb can be diagnosed by varying the dosage of the adsorbent. MCP (0.5) was modified into gel PMCP with 0.1, 0.25, 0.5, and 1 of its weight percent. 100 mL of 10ppm solution of the Congo Red (CR) dye was used as a dye pollutant. It was observed that 1% PMCP was able to adsorb around 99.44% followed by 90.80, 76.94, and 76.81 % of 0.5, 0.25, and 0.1 respectively. The high percent removal can be attributed to the increase in surface functionalities of the composite enhancing the adsorption property for the removal of pollutants. Figure 4.11 shows the change in removal efficiency with an increase in adsorbent dosage.

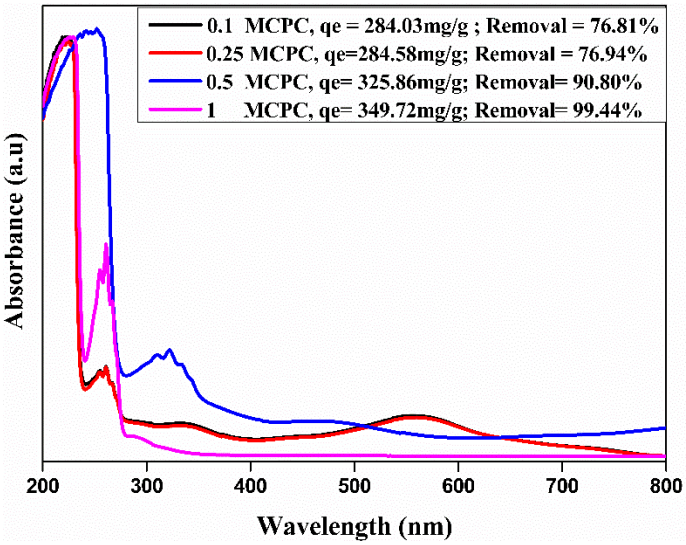

Figure 4.11 UV-Visible spectrum depicting the effect of adsorbent dosage at 30 ºC

4.3.3.2 Effect of dye concentration

An increase in the concentration of dye results in the determination of maximum adsorbency by the adsorbent. Figure 4.12 shows varying dye concentrations from 10ppm to 50ppm with their removal percentage. Owing to the presence of adsorption sites, the adsorbent was able to remove 99 % of Congo red (CR) maintaining its consistency up to 50ppm. This constant trend suggests that the adsorbent is capable of removing dye molecules from polluted sources with increased concentration.

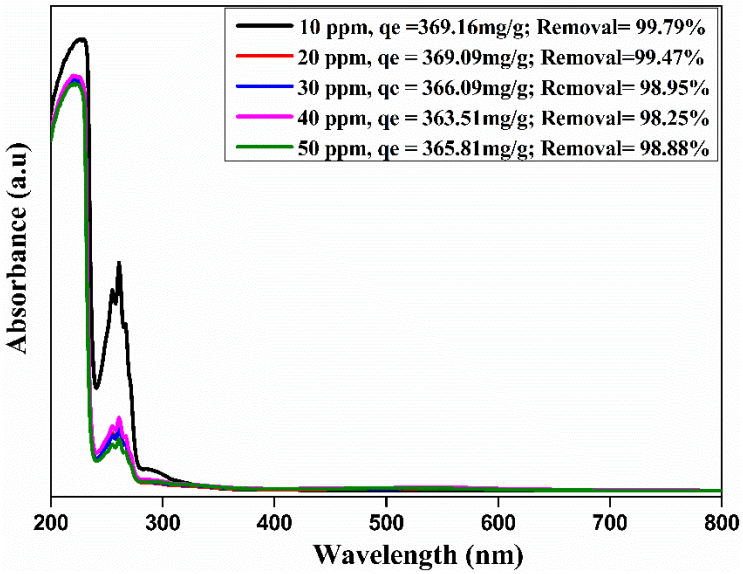

Figure 4.12 UV-Visible spectrum depicting the effect of dye concentrations at 30 ºC

4.3.3.3 Effect of pH

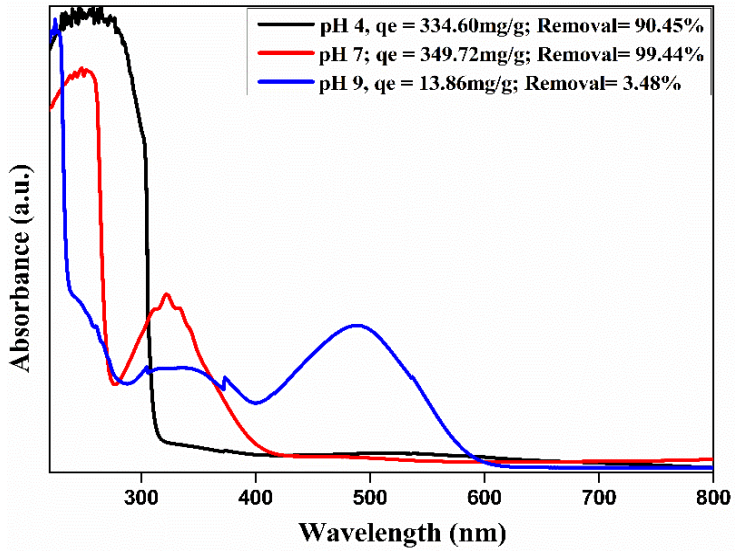

Figure 4.13 UV-Visible spectrum depicting the effect of pH at 30 ºC

The adsorbent's efficiency at different pH was studied to observe the adsorption behavior. With the decrease in pH medium (pH=3), the PAni in the composite transforms to emeraldine salt form with an increase in protonation of the sulfonate group present.

This results in an increase in dye adsorption due to electrostatic interaction. With an increase in pH medium (pH=9), the PAni changes to an emeraldine base. This base form and the negatively charged sulfonate group of the CR dye repel each other lowering the adsorption efficiency. At neutral pH=7, dye molecules remain in a deprotonated state which results in strong interaction between PAni and SO_3^- group increasing the adsorption capacity at a neutral medium. Hence all the required analyses for the adsorption were carried out at pH=7. The study of different pH was observed in Figure 4.13.

4.3.3.4 Effect of Contact Time

The adsorbency of the sorbate on the sorbent was determined by investigating the effect of time at different intervals. 0.1gm of the sorbent was used in 20ppm of 100mL dye solution. A removal percentage of 51.18% was observed in the first 5min of contact. With the increase in the effect of time, removal efficiency increases up to 76.74% in 120 min, 83.91% in 180min, and 92.06% in 240min finally attaining equilibrium at 300 min with 99.44% removal as the active sites were completely adsorbed by the dye molecules (Figure 4.14). The rate of adsorption accelerated as soon as it came into contact with sorbent within the first 5 minutes due to the presence of convenient sites.

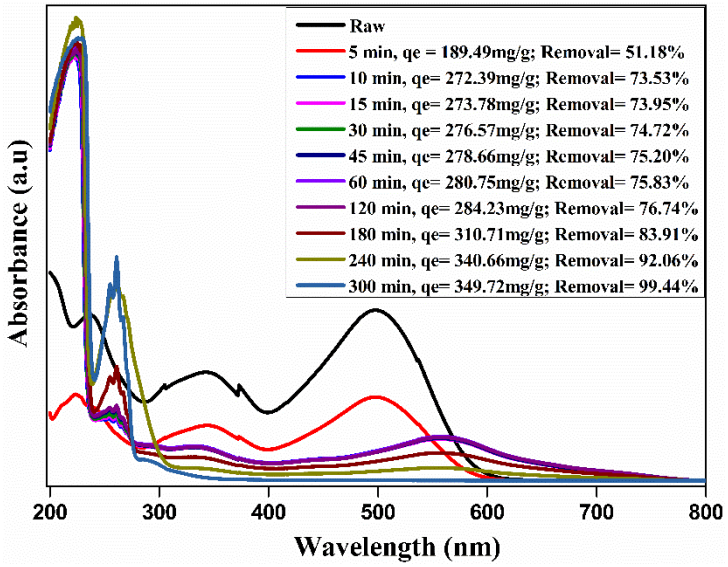

Figure 4.14 UV-Visible spectrum depicting the effect of contact time at 30 ºC

4.3.3.5 Selective mixture of dyes

Discharge of textile effluents includes the presence of both cationic as well as anionic dyes. To observe the selectivity of the adsorbent for use in practical applications, the sorbent was exposed to a mixture of dyes. Three cationic dyes Crystal violet (CV), Acridine orange (AO), and Malachite green (MG) were prepared and mixed with CR in a

1:1 ratio to form a binary solution. From the UV spectra in Figure 4.15(a-c). the sorbent was able to effectively remove CR dye from the mixture of three separate dye solutions with around adsorption of 94.80, 91.79, and 96.73% from CR-CV, CR-AO, and CR-MG mixture solutions. Further, the sorbent even observed complete and partial removal of AO (99%) and CV (72.10%) dye from the mixture within 5 hours. Thus, the adsorbent can be utilized as an effective material for the adsorption and removal of a mixture of dyes from polluted water sources.

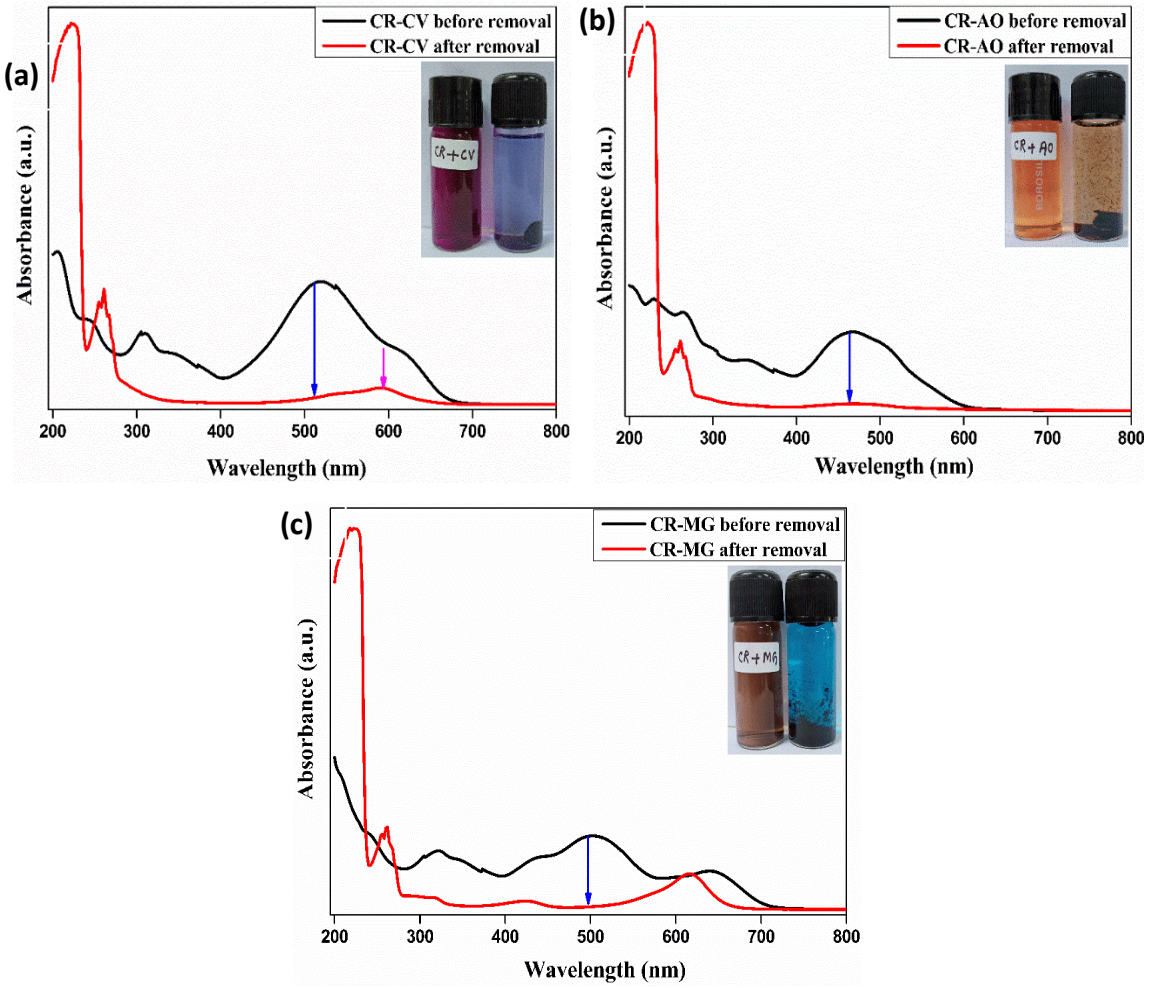

Figure 4.15 UV-Visible spectral evolution of dye mixture (a) CR-CV (b) CR-AO (c) CR-MG and their removal at 30 ºC for 300min

4.3.3.6 Adsorbent reusability

For use in large-scale industrial applications, the reduction of waste remnants holds significant importance. Here, 0.1gm of the sorbent was dipped in 100mL of 20ppm CR solution. After adsorption, the analyte was analyzed via UV-Vis spectroscopy while the same sorbent was used to adsorb another 100mL of dye solution. A total of 5 consecutive cycles was observed as shown in Figure 4.16(a). With each cycle, a slight decrease in adsorption percent was evident with 99.86% in 1st cycle to 82.93% in 5th

cycle. The decrease in percent absorbance is apparently due to the precedent dye molecules on the sorbent surface. Thus, the results convey the effectual dye removal up to nearly 83% even in the 5th cycle proving advantageous for use in the industrial sector (Figure 4.16b).

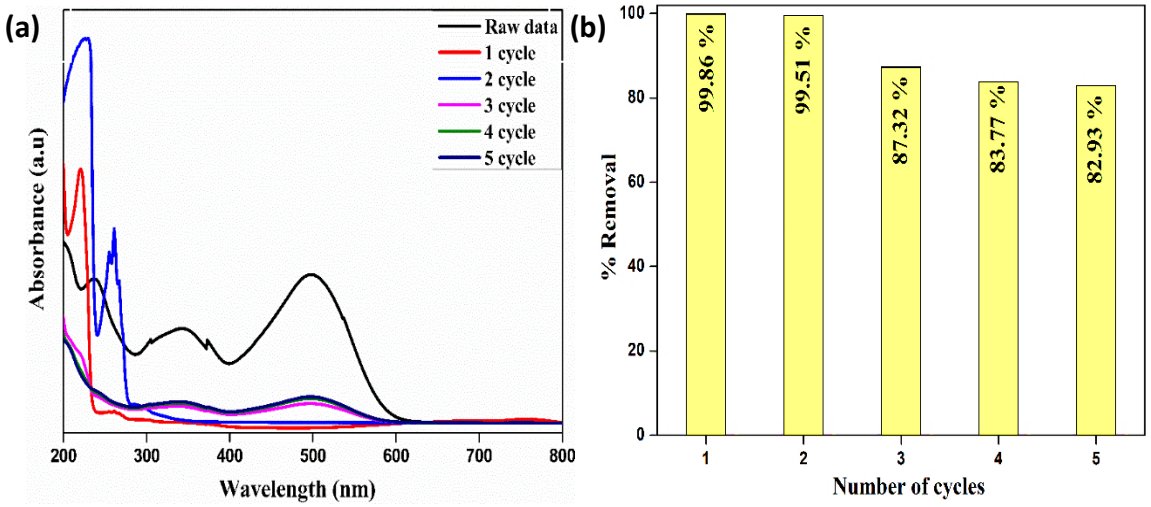

Figure 4.16 (a) UV-Visible spectral evolution of recyclability study of CR dye, (b) Reusability bar graph of CR dye

4.3.3.7 Adsorption Kinetics

To interpret the mechanism of dye adsorption, kinetic plots were studied concerning time concerning adsorption by the sorbent. The plot of t/q_t vs. time for pseudo-second-order kinetic observed a linear fit curve for kinetic models. While the correlation coefficient perceived an R^2 value of 0.99 providing a better fit than that of the first-order kinetic model acting as the limiting step between sorbent and CR molecules.

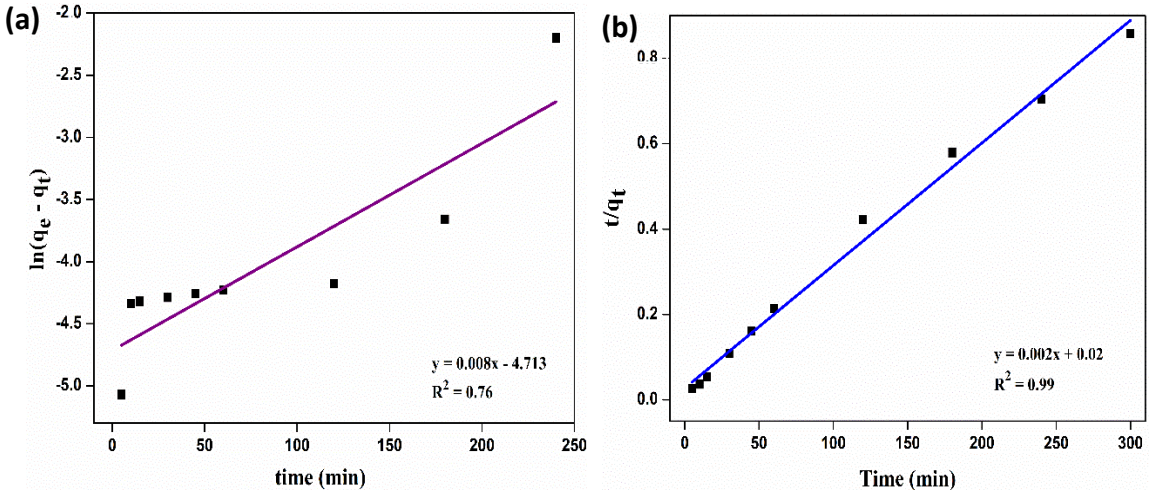

Figure 4.17 (a) The plot of $\ln(qe-q_t)$ vs time for first order kinetics and (b) plot of t/q_t vs time graph for second order kinetics involved in dye adsorption

Thus, the dye adsorption mechanism was found to follow the chemisorption process behavior. The fitting curve and all the data values for k_1 and k_2 are shown in Figure 4.17 and Table 4.6.

Table 4.6 Kinetic model parameters from dye adsorption

pseudo-first-order kinetics model		pseudo-second-order kinetics model		
$k_1(min^{-1})$	R^2	$k_2(gg^{-1}min^{-1})$	$Q_{max}(gg^{-1})$	R^2
0.301×10^{-3}	**0.76**	0.289×10^{-3}	0.86	**0.99**

4.3.3.8 Adsorption Isotherm

An Isotherm study was carried out to determine the interacting nature between sorbent and adsorbate at equilibrium. Two well-known isotherm models, Langmuir and Freundlich were used to analyze the adsorption studies. The linear fit curves for both models have been shown in Figure 4.18 and Table 4.7.

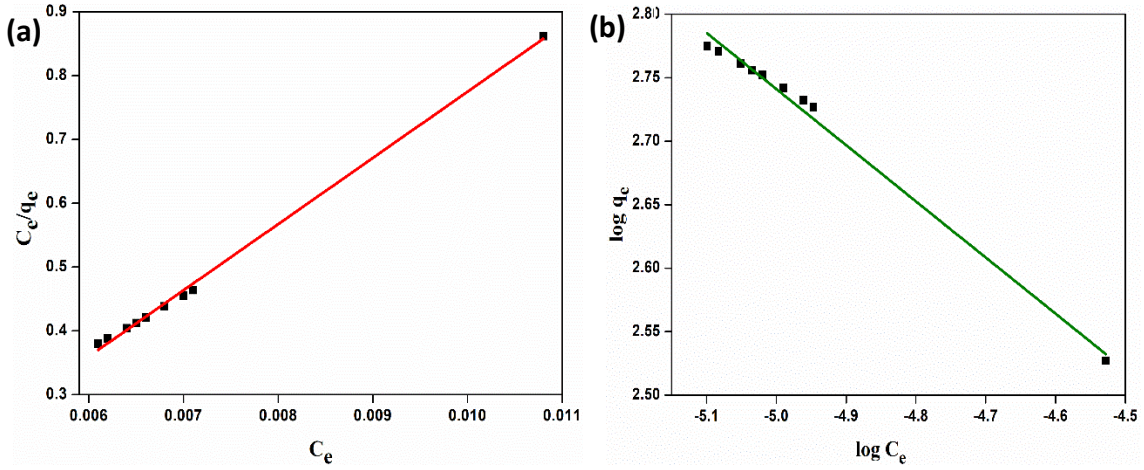

Figure 4.18 Adsorption isotherm of (a) plot Ce/qe vs Ce (Langmuir), (b) plot of log qe vs log Ce (Freundlich) for adsorbed dye

.

It can be seen that both the curves obtained were linearly fitted however the regression coefficient observed by the Langmuir model has a value of 0.997 which is higher than the Freundlich model (0.991). Langmuir model also observed a separation factor (R_L) around 0.76 which confirms the favorable adsorption process. The maximum adsorption capacity was found to be 349.72mg/g. Thus, from the above results, it can be concluded that adsorption between dye and sorbent follows chemisorption behavior with monolayer deposition on the sorbent's homogeneous surface.

Table 4.7 Parameters for adsorption isotherm from CR dye adsorption

ISOTHERMS & PARAMETERS	Langmuir Isotherm				Freundlich Isotherm		
	q_e (mgg^{-1})	K_L (L/mg)	R_L	R^2	1/n	K_F (mgg^{-1})	R^2
	349.72	0.103	0.76	**0.997**	2.26	0.529	0.991

4.3.3.9 Intra-particle diffusion study

The mass transfer or diffusion model by Weber and Morris was followed to understand the mechanism of adsorption of dyes from the aqueous phase to the adsorbent. As observed from the qt vs $t^{1/2}$ graph in Figure 4.19, the diffusion plot staged a three-step sorption process. A steady rise observed in the first step signifies the diffusion process by CR molecules from the solution to the external surface of the sorbent. The second step denotes the infusion of dye molecules to the interior area of the sorbent until it attains maximum adsorption in the third step where the pores are accumulated by dye molecules as it reaches the equilibrium position. The rate of diffusion along with the thickness of the layer was found to be 0.355 and 262.11mg/g (Table 4.8).

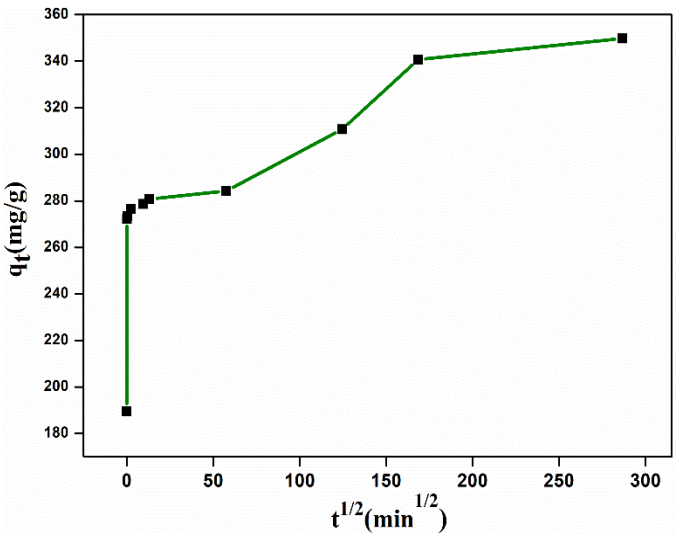

Figure 4.19 Intra-particle diffusion plot of qt vs $t^{1/2}$ for CR dye

Table 4.8 Parameters for Weber-Morris model of dye adsorption

INTRA-PARTICLE DIFFUSION	PARAMETERS		
	k_{id}	C	R^2
CR dye	0.355	262.11	0.57

4.3.3.10 Mechanism of adsorption

The mechanism of dye adsorption involves physical and chemical interactions due to the presence of functional groups or the surface structure. MMT was used as one of the raw materials due to the presence of its large surface area and mesoporous structure. The possible mechanisms occurring during interaction of dye molecules and adsorbent may involve the following routes: With the addition of PAni chains in between the silicate ions, the sulfonic group of the dye interacts with N^+H electrostatically. π–π interaction occur between the double bonds of the aromatic rings present in the dye as well as PAni (Scheme 4.3) Formation of H-bonding between NH_2 group of Congo red and hydroxyl group of Polyvinyl alcohol is another possible mechanism.

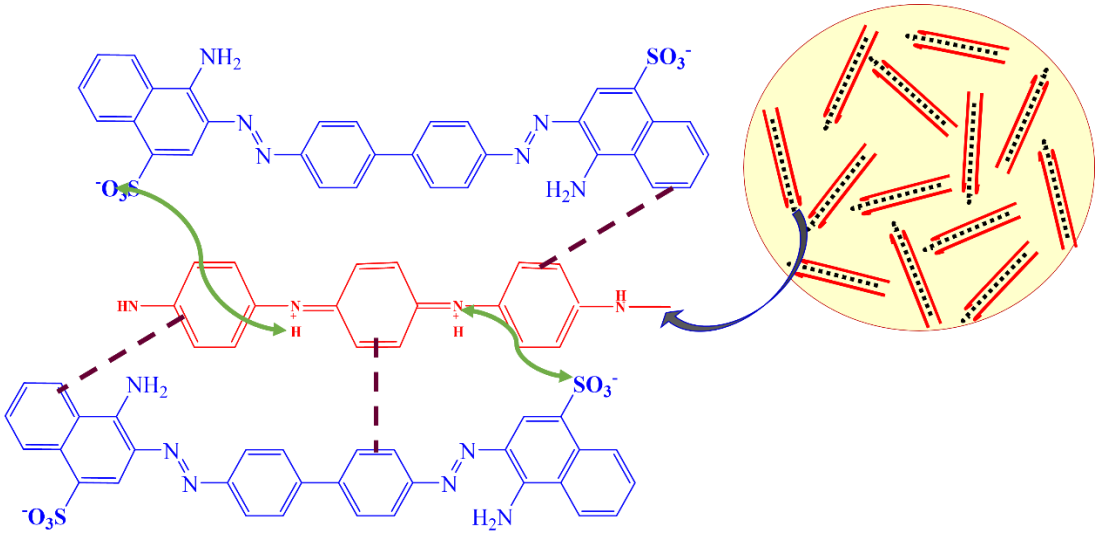

Scheme 4.3 Mechanistic pathway of the interaction between PMCP organogel and congo red dye

The physicochemical properties of the gel influence the behavioral aspect of interaction with the dye solution and retaining molecules. Inclusion of clay material provides surface area in addition to providing active sites with pore sizes which immensely enhances the rate of adsorption. The presence of functional groups as amine, imine with hydroxyl groups binds with the dye molecules through electrostatic interaction as well as H-bonding. Further, the charges present in amine, and imine groups help highly in the effective removal of negatively charged dyes. The stability of the gel to perform under different pH along with regeneration ability for multiple adsorption cycles are a few of the physicochemical characteristics increasing the performance of the adsorption.

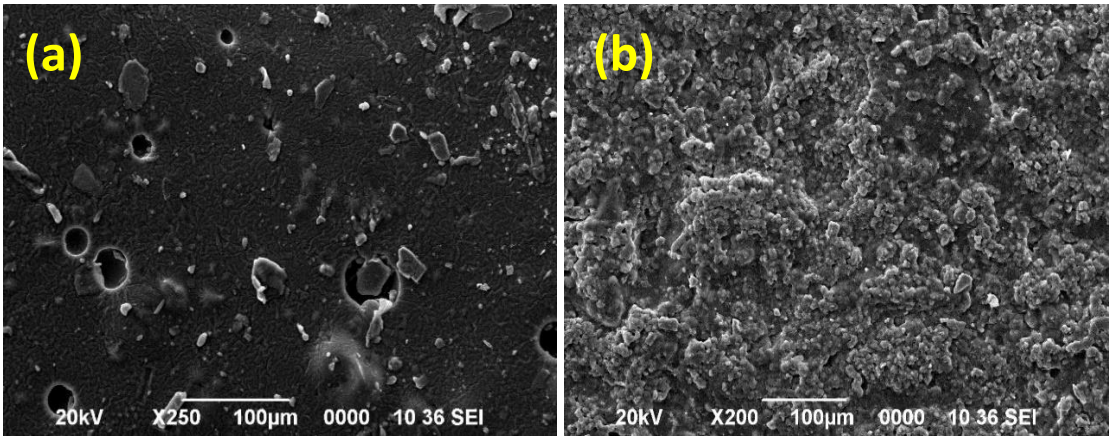

Figure 4.20 SEM micrographs of PMCP gel (a) before dye adsorption (b) after dye adsorption

The presence of micropores (obtained from the BET study) helps in filling up pores by diffusing the dye molecules on the surface of the adsorbent. This can be evident from SEM morphological study (Figure 4.20a-b) where a rough surface with an accumulation of certain pores was seen visible before the adsorption. After the adsorption of the dye, it was observed that the dye particles deposited all over the surface area of the gel.

The removal of CR dye by the present study, prepared organogel (PMCP) was compared with that of other adsorbents concerning time, removal percentage, and adsorption capacity which has been charted in Table 4.9.

Table 4.9 Adsorptive study on Congo Red removal by different adsorbents

Type of adsorbent	Adsorption capacity (mg/g)	% Removal	Reference
Chitosan/MMT nanocomposite	54.52		[39]
pTSA doped PAni@GO-MWCNT composite	56.7		[40]
Poly(AA-co-hydroxyethyl methacrylate) and Na alginate	90	97.6%	[41]
Metal organic gels of catechol based ligands – MOG1 MOG2		86.43% 95.20%	[24]
Nano zerovalent Mn/biochar composite	117.64	77%	[42]
PPy multiwalled nanocomposite	147	98%	[43]
Amine functionalized magnetic iron oxide nanoparticles	183.15	99%	[44]
PAni-NT	194	98%	[32]

MgO-GO composite microspheres	237		[45]
Super magnetic graphene/PAni/Fe_3O_4 nanocomposite	248.76	92.4%	[46]
Insitu chemical polymerization of Aniline Pyrrole	250.01 66.66		[47]
Ferrocene based mesoporous material	312.5		[48]
PVA (MMT/PAni composite) organogels	349.72	99.44%	This work
Porous NiO-Al_2O_3 nanocomposite	357		[49]
Porous ZnO-Al_2O_3 microspheres	397		[50]

4.4 CONCLUSION

Through this work, the preparation and characterization of an organogel that employs a hybrid composite consisting of MMT and PAni have been examined. The gel has been designed to effectively absorb the pores from the MMT and utilize surface enhancement by PAni to remove highly toxic carcinogenic pollutant Chloroform as well as organic dyes from polluted water sources. Our results indicated that the gel-based sorbent was capable of absorbing chloroform up to 20 times its weight while removing up to 99% of CR dye with maximum adsorption of 349.72 mg/g. Our study revealed that the sorbent followed monolayer adsorption by Langmuir isotherm, accompanied by a pseudo-second-order kinetics mechanism, with the diffusion model serving as one of the rate-determining processes. The mechanism of the dye adsorption involved key interactions including electrostatic, π-π as well as H-bonding. Moreover, the organogel displayed selectivity among a mixture of dyes with excellent reusability properties retaining up to 83% even in the 5th cycle. The current work involves the preparation of organogel from economic materials found conveniently proved to be useful for industrial usage with satisfactory results thus holding as a promising material for the removal of organic pollutants from wastewater.

4.5 REFERENCES

[1] Drumond Chequer, F. M., Oliveira, G. A. R., Anastacio Ferraz, E. R., Carvalho, J., Boldrin Zanoni, M. V., and Oliveir, D.P. Textile Dyes: Dyeing Process and Environmental Impact, in: *Eco-Friendly Textile Dyeing and Finishing*. InTech, 2013.

[2] Methneni, N., González, J. A. M., Jaziri, A. H., Mansour, B., and Serrano, M. F. Persistent organic and inorganic pollutants in the effluents from the textile dyeing industries: Ecotoxicology appraisal via a battery of biotests. *Environmental Research*, 196, 110956, 2021.

[3] Bharagava, R. N., Saxena, G., and Mulla, S. I. Introduction to Industrial Wastes Containing Organic and Inorganic Pollutants and Bioremediation Approaches for Environmental Management. In *Bioremediation of Industrial Waste for Environmental Safety*, pages 1–18. Springer Singapore, 2020.

[4] Michalowicz, J., and Duda, W. Phenols – Sources and Toxicity. *Polish Journal pf Environment Studies*, 16 (3): 347-362, 2007.

[5] Ahlborg, U. G., Thunberg, T. M., and Spencer, H.C. Chlorinated Phenols: Occurrence, Toxicity, Metabolism, and Environmental Impact, *CRC Critical Reviews in Toxicology*, 7 (1): 1-35, 1980.

[6] Bhatia, D., Sharma, N. R., Singh, J., and Kanwar, R.S. Biological methods for textile dye removal from wastewater: A review. *Critical Review in Environment Science Technology*, 47: 1836–1876, 2017.

[7] Nidheesh, P. V., Zhou, M., and Oturan, M. A. An overview on the removal of synthetic dyes from water by electrochemical advanced oxidation processes. *Chemosphere*, 197: 210–227, 2018.

[8] Hassan, M. M., and Carr, C. M. A critical review on recent advancements of the removal of reactive dyes from dyehouse effluent by ion-exchange adsorbents. *Chemosphere*, 209: 201–219, 2018.

[9] Li, W., Zhang, Y., Liu, T., Huang, J., and Wang, Y. Comparison of ion exchange and solvent extraction in recovering vanadium from sulfuric acid leach solutions of stone coal. *Hydrometallurgy*, 131: 1–7, 2013.

[10] Wei, Y., Cheng, X., Ding, A., and Xu, J. Magnesium Silicate Polymer as a Coagulant for Reactive Dye Removal from Wastewater: Considering the Intrinsic pH in Magnesium Silicate Polymer and Coagulation Behavior. *ACS Omega*, 5 (40): 26094-26100, 2020.

[11] Marchetti, P., Solomon, M. F. J., Szekely, G. and Livingston, A. G. Molecular separation with organic solvent nanofiltration: A critical review. *Chemical Reviews*, 114 (21): 10735–10806, 2014.

[12] Muruganandham, M., and Swaminathan, M. Photochemical oxidation of reactive azo dye with UV-H2O2 process. *Dyes and Pigments*, 62 (3): 269–275, 2004.

[13] Ince, N. H. ``Critical'' Effect of Hydrogen Peroxide in Photochemical Dye Degradation. *Water Research*, 33 (4): 1080-1084, 1999.

[14] Gisi, S. D., Lofrano, G., Grassi, M., and Notarnicola, M. Characteristics and adsorption capacities of low-cost sorbents for wastewater treatment: A review. *Sustainable Materials and Technologies*, 9: 10–40, 2016.

[15] Yati, I., Karadag, K., and Sonmez, H. B. Amphiphilic poly(ethylene glycol) gels and their swelling features. *Polymers Advanced Technologies*, 26 (6): 635–644, 2015.

[16] Lim, J. Y. C., Goh, S. S., Liow, S. S., Xue, K., and Loh, X. J. Molecular gel sorbent materials for environmental remediation and wastewater treatment. *Journal of Materials Chemistry A*, 7: 18759–18791, 2019.

[17] Baruah, K., Dutta, R., Doley, S., and Dolui, S. K. Grafted polymeric organogel using low molecular weight gelator as an effective medium for expulsion and purification of cationic dyes and organic pollutants from contaminated surface water. *European Polymer Journal*, 195: 112213, 2023.

[18] Sridhar, S. P., John, J., Holmqvist, P., Olsson, U., Chandran, S., and Joseph, B. Adsorption of anionic dyes using a poly(styrene-block-4-vinylpyridine) block copolymer organogel. *Langmuir*, 37: 3996-4006, 2021.

[19] Das, S., Chakraborty, P., Ghosh, R., Paul, S., Mondal, S., Panja, A., and Nandi, A. K. Folic Acid-Polyaniline Hybrid Hydrogel for Adsorption/Reduction of Chromium(VI) and Selective Adsorption of Anionic Dye from Water. *ACS Sustainable Chemical Engineering*, 5 (10): 9325–9337, 2017.

[20] Zhu, S., Qu, T., Irshad, M. K., and Shang, J. Simultaneous removal of Cd(II) and As(III) from co-contaminated aqueous solution by α-FeOOH modified biochar. *Biochar*, 2 (1): 81–92, 2020.

[21] Bhat, S., Uthappa, U. T., Sadhasivam, T., Altalhi, T., Soo Han, S., and Kurkuri, M. D. Abundant cilantro derived high surface area activated carbon (AC) for superior adsorption performances of cationic/anionic dyes and supercapacitor application. *Chemical Engineering Journal*, 459, 141577, 2023.

[22] Srivastava, A., Gupta, B., Majumder, A., Gupta, A. K., and Nimbhorkar, S. K. A comprehensive review on the synthesis, performance, modifications, and regeneration of activated carbon for the adsorptive removal of various water pollutants. *Journal of Environmental Chemical Engineering*, 9 (5), 106177, 2021.

[23] V. Hegde, U.T. Uthappa, M. Suneetha, T. Altalhi, S. Soo Han, M.D. Kurkuri, Functional porous Ce-UiO-66 MOF@Keratin composites for the efficient adsorption of trypan blue dye from wastewater: A step towards practical implementations. *Chemical Engineering Journal*, 461, 142103, 2023.

[24] Hong, Y., Gao, Z., Chen, M., Hao, J., and Dong, S. Metal-Organic Gels of Catechol-Based Ligands with Ni(II) Acetate for Dye Adsorption. *Langmuir*, 34 (32): 9435-9441, 2018.

[25] Dutta, S., Srivastava, S. K., Gupta, B., and Gupta, A. K. Hollow polyaniline microsphere/MnO2/Fe3O4nanocomposites in adsorptive removal of toxic dyes from contaminated water. *ACS Applied Material Interfaces*, 13 (45): 54324–54338, 2021.

[26] Chen, B., Evans, J. R. G., Greenwell, H. C., Boulet, P., Coveney, P. V., Bowden, A. A., and Whiting, A. A critical appraisal of polymer–clay nanocomposites. *Chemical Society Reviews*, 37 (3): 568–594, 2008.

[27] Aljar, M. A. A., Rashdan, S., and El-Fattah, A. A. Environmentally friendly polyvinyl alcohol−alginate/ bentonite semi-interpenetrating polymer network nanocomposite hydrogel beads as an efficient adsorbent for the removal of methylene blue from aqueous solution. *Polymer*, 13 (22), 4000, 2021.

[28] Park, Y., Ayoko, G. A., Horváth, E., Kurdi, R., Kristof, J., and Frost, R. L. Structural characterisation and environmental application of organoclays for the removal of phenolic compounds. *Journal of Colloid and Interface Science*, 393 (1): 319–334, 2013.

[29] Park, Y., Ayoko, G. A., and Frost, R. L. Characterisation of organoclays and adsorption of p-nitrophenol: Environmental application. *Journal of Colloid and Interface Science*, 360 (2): 440–456, 2011.

[30] Pandey, P., and Saini, V. K. Pillared interlayered clays: sustainable materials for pollution abatement. *Environmental Chemistry Letters*, 17: 721–727, 2019.

[31] Tian, S., Jiang, P., Ning, P., and Su, Y. Enhanced adsorption removal of phosphate from water by mixed lanthanum/aluminum pillared montmorillonite. *Chemical Engineering Journal*, 151 (1-3): 141–148, 2009.

[32] Mondal, S., Rana, U., Das, P., and Malik, S. Network of Polyaniline Nanotubes for Wastewater Treatment and Oil/Water Separation, *ACS Applied Polymer Materials*, 1 (7): 1624–1633, 2019.

[33] Vilela, S. O., Soto-Oviedo, M. A., Albers, A. P. F., and Faez, R. Polyaniline and Mineral Clay-based Conductive Composites. *Materials Research*, 10 (3): 297-300, 2007.

[34] Narayanan, B. N., Koodathil, R., Gangadharan, T., Yaakob, Z., Saidu, F. K., and Chandralayam, S. Preparation and characterization of exfoliated polyaniline/montmorillonite nanocomposites. *Materials Science and Engineering: B*, 168, (1): 242–244, 2010.

[35] Kazim, S., Ahmad, S., Pfleger, J., Plestil, J., and Joshi, Y. M. Polyaniline-sodium montmorillonite clay nanocomposites: Effect of clay concentration on thermal, structural, and electrical properties. *Journal of Materials Science*, 47 (1): 420–428, 2012.

[36] Mody, H. M., Oza, P. M., and Pandya, V. P. Alumina-pillared clay of improved thermal stability. *Applied Clay Science*, 8 (1): 53-60, 1993.

[37] Abolghasemi, M. M., Parastari, S., and Yousefi, V. Microextraction of phenolic compounds using a fiber coated with a polyaniline-montmorillonite nanocomposite. *Microchimica Acta*, 182 (1-2): 273–280, 2015.

[38] Zheng, S., Sun, Z., Park, Y., Ayoko, G. A., and Frost, R. L. Removal of bisphenol A from wastewater by Ca-montmorillonite modified with selected surfactants. *Chemical Engineering Journal*, 234: 416–422, 2013.

[39] Wang, L., and Wang, A. Adsorption characteristics of Congo Red onto the chitosan/montmorillonite nanocomposite. *Journal of Hazardous Materials*, 147 (3): 979–985, 2007.

[40] Ansari, M. O., Kumar, R., Ansari, S. A., Ansari, S. P., Barakat, M. A., Alshahrie, A., and Cho, M. H. Anion selective pTSA doped polyaniline@graphene oxide-multiwalled carbon nanotube composite for Cr(VI) and Congo red adsorption. *Journal of Colloid and Interface Science*, 496: 407–415, 2017.

[41] Mandal, B., and Ray, S. K. Synthesis of interpenetrating network hydrogel from poly(acrylic acid-co-hydroxyethyl methacrylate) and sodium alginate: Modeling and kinetics study for removal of synthetic dyes from water. *Carbohydrate Polymers*, 98 (1): 257–269, 2013.

[42] Iqbal, J., Shah, N. S., Sayed, M., Niazi, N. K., Imran, M., Khan, J. A., Khan, Z. U. H., Hussien, A. G. S., Polychronopoulou, K., and Howari, F. Nano-zerovalent manganese/biochar composite for the adsorptive and oxidative removal of Congo-red dye from aqueous solutions. *Journal of Hazardous Materials*, 403, 123854, 2021.

[43] Aliabadi, R. S., and Mahmoodi, N. O. Synthesis and characterization of polypyrrole, polyaniline nanoparticles and their nanocomposite for removal of azo dyes; sunset yellow and Congo red. *Journal of Cleaner Production*, 179: 235–245, 2018.

[44] Sahoo, J. K., Paikra, S. K., Mishra, M., and Sahoo, H. Amine functionalized magnetic iron oxide nanoparticles: Synthesis, antibacterial activity and rapid removal of Congo red dye. *Journal of Molecular Liquids*, 282: 428–440, 2019.

[45] Xu, J., Xu, D., Zhu, B., Cheng, B., and Jiang, C. Adsorptive removal of an anionic dye Congo red by flower-like hierarchical magnesium oxide (MgO)-graphene oxide composite microspheres. *Applied Surface Science*, 435: 1136–1142, 2018.

[46] Mu, B., Tang, J., Zhang, L., and Wang, A. Facile fabrication of superparamagnetic graphene/polyaniline/Fe3O4 nanocomposites for fast magnetic separation and efficient removal of dye. *Scientific Reports*, 7 (1), 5347, 2017.

[47] Chafai, H., Laabd, M., Elbariji, S., Bazzaoui, M., and Albourine, A. Study of congo red adsorption on the polyaniline and polypyrrole. *Journal of Dispersion Science and Technology*, 38 (6): 832–836, 2017.

[48] Kaur, S., Rani, S., Kumar, V., Mahajan, R. K., Asif, M., Tyagi, I., and Gupta, V. K. Synthesis, characterization and adsorptive application of ferrocene based mesoporous material for hazardous dye Congo red. *Journal of Industrial and Engineering Chemistry*, 26: 234–242, 2015.

[49] Lei, C., Zhu, X., Le, Y., Zhu, B., Yu, J., and Ho, W. Hierarchically porous NiO-Al2O3 nanocomposite with enhanced Congo red adsorption in water. *RSC Advances*, 6 (13): 10272–10279, 2016.

[50] Lei, C., Pi, M., Xu, D., Jiang, C., and Cheng, B. Fabrication of hierarchical porous ZnO-Al 2 O 3 microspheres with enhanced adsorption performance. *Applied Surface Science*, 426: 360–368, 2017.